Spin relaxation and spin Hall transport in 5*d* transition-metal ultrathin films

Nguyen H. Long,* Phivos Mavropoulos,† Bernd Zimmermann, David S. G. Bauer, Stefan Blügel, and Yuriy Mokrousov
Peter Grünberg Institut and Institute for Advanced Simulation, Forschungszentrum Jülich and JARA, D-52425 Jülich, Germany
(Received 9 May 2014; revised manuscript received 23 July 2014; published 7 August 2014)

The spin relaxation induced by the Elliott-Yafet mechanism and the extrinsic spin Hall conductivity due to the skew scattering are investigated in 5*d* transition-metal ultrathin films with self-adatom impurities as scatterers. The values of the Elliott-Yafet parameter and of the spin-flip relaxation rate reveal a correlation with each other that is in agreement with the Elliott approximation. At 10-layer thickness, the spin-flip relaxation time in 5*d* transition-metal films is quantitatively reported about few hundred nanoseconds at atomic percent. This time scale is one and two orders of magnitude shorter than the values in Au and Cu thin films, respectively. The anisotropy effect of the Elliott-Yafet parameter and of the spin-flip relaxation rate with respect to the direction of the spin-quantization axis in relation to the crystallographic axes is also analyzed. We find that the anisotropy of the spin-flip relaxation rate is enhanced due to the Rashba surface states on the Fermi surface, reaching values as high as 97% in 10-layer Hf(0001) film or 71% in 10-layer W(110) film. Finally, the spin Hall conductivity as well as the spin Hall angle due to the skew scattering off self-adatom impurities are calculated using the Boltzmann approach. Our calculations employ a relativistic version of the first-principles full-potential Korringa-Kohn-Rostoker Green function method.

DOI: 10.1103/PhysRevB.90.064406 PACS number(s): 72.25.Rb, 73.50.Bk, 72.25.Ba, 85.75.−d

I. INTRODUCTION

Spin-dependent transport phenomena in nanoscale structures such as metallic thin films attract wide attention in spintronics where the spin degree of freedom is manipulated for data transfer and storage in information technology [1–3]. Due to spin-orbit coupling (SOC), an injected spin polarization in a metal decays exponentially in time as $\exp(-t/T_{\mathrm{sf}})$, where T_{sf} is the spin-flip relaxation time. Therefore, understanding and manipulating the spin-relaxation processes is one of the essential conditions for practical applications [3–5]. To give two practical examples, in spin-information devices the spin-flip relaxation time is usually required to be large [6]. On the contrary, in ultrafast magnetization reversal devices, a short spin-relaxation time is necessary [7]. Spin-orbit-induced scattering processes in metals are also at the origin of the spin Hall effect (SHE) [8–12], where a spin current is detected in the direction perpendicular to an applied electric field, or the inverse spin Hall effect (ISHE) [13,14], where a spin current, injected into a nonmagnetic metal, induces a transverse charge current. The SHE and ISHE have become effective ways for spin current manipulation and detection in nanodevices.

It is well established that the Elliott-Yafet mechanism [15,16] of spin-flip scattering plays the most important role in metals with time-reversal symmetry [17] (i.e., nonmagnetic) and space-inversion symmetry. Owing to the presence of spin-orbit coupling, the Bloch wave functions are superpositions of the spin-up and -down states which allow a spin-flip scattering off impurities at low temperatures or off phonons at high temperatures even if the scattering potential is spin diagonal. In the Elliott approximation, after neglecting the form of the scattering potential, the spin-flip relaxation rate T_{sf}^{-1} is estimated to be proportional to the spin-mixing, or Elliott-Yafet parameter (EYP) b^2.

The Elliott-Yafet spin-relaxation mechanism and the spin Hall current induced by the scattering off impurities in bulk metals have been already investigated within models as well as by first-principles calculations [18–25]. However, little is known about these effects in metallic thin films with thickness in the nanometer regime. In these systems, owing to the breaking of translational symmetry in the direction perpendicular to the film, many parameters have to be taken into account, such as the thickness and the crystalline orientation of the films. Importantly, Rashba surface states [26,27] can be formed around the Fermi level and they were shown to enhance the spin-flip relaxation rate [23,28,29]. Thin film is a keyword for reducing the size of spintronics devices. It also gives a flexibility in manipulating electron spins in the spin Hall experiments.

In previous works [29,30], we have investigated in depth the spin-relaxation mechanism in noble-metal and W(001) ultrathin films. Our calculations revealed spin-relaxation mechanisms that were brought about by the reduced dimensionality and that would not be present in the bulk of these metals. For one thing, we found [30] that the free-electron-like Fermi surface of the noble metals, when projected in the surface Brillouin zone of the ultrathin film, cuts through the Brillouin zone edge producing spin-flip hot spots that have only been reported in the case of multivalent metals [18] so far. Additionally, we analyzed the surface states in the case of W(001) films [29] and found that the Rashba character can strongly contribute to spin relaxation; we also saw an oscillatory behavior of the spin relaxation as a function of the film thickness. In both cases [29,30], we also found a considerable anisotropy of the EYP as well as spin-relaxation rate with respect to the angle between the injected spin polarization and the film normal.

In this work, we extend our computational study to a number of metallic systems, namely, ultrathin films of 5*d* metals as well as Au and Cu with different typical surface orientations: i.e., (111) and (001) for fcc, (001) and (110) for bcc, and (0001) for hcp structures. Our focus on 5*d* metals is motivated by their

*h.nguyen@fz-juelich.de
†ph.mavropoulos@fz-juelich.de

 ©2014 American Physical Society

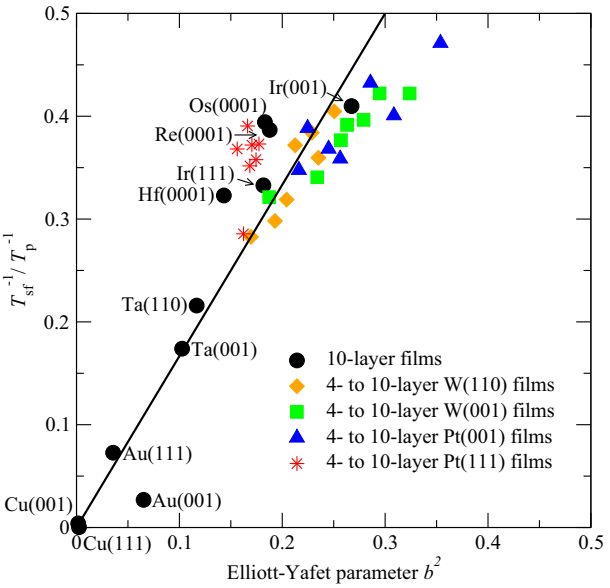

FIG. 1. (Color online) Comparison between the ratio of the spin-flip rate and the momentum-relaxation rate for transition-metal films with self-adatom impurities and the Elliott-Yafet parameter. The solid black line is the function $f(x) = 1.6x$ (fit by least squares) and serves as a guide to the eye.

strong SOC. It is also well known that the 5*d* transition-metal surfaces such as Pt, Ir, or W are frequently used as substrates for growth of 3*d* magnetic thin films [31–34], while Cu, Pt, or Au are frequently used as conducting contacts or spin Hall probes in spintronics experiments [11,14,35]. For the aforementioned systems, we report on the calculation of the Elliott-Yafet parameter, the spin-flip relaxation rate in the presence of defect-induced electron scattering, and its anisotropy. Comparison among different systems reveals that the spin-flip relaxation rate, and in particular its anisotropy, has a spread of more than an order of magnitude. This is a possibly unexpected finding since the 5*d* systems are characterized by comparable SOC strength and, to a crude approximation, by similarly dense bands in the vicinity of the Fermi level. Additionally, we find that the Elliott approximation to the spin-flip relaxation rate, that is sometimes considered crude as it neglects the form of the scattering potential, is qualitatively good in most cases. We stress this finding by demonstrating it already in Fig. 1 where the ratio between spin flip and momentum-relaxation rate $T_{\rm sf}^{-1}/T_{\rm p}^{-1}$ is plotted against the EYP for a number of systems; these results are discussed in detail in Sec. III. Furthermore, we present calculations of the spin Hall angle due to the extrinsic skew scattering off defects. This, too, can change in magnitude but also in sign depending on the material, on the film thickness, and even on the surface orientation, revealing the high complexity of the involved scattering processes.

II. THEORY

The calculation of the electronic structure is done within the local density approximation to density-functional theory in the parametrization by Vosko *et al.* [36]. We employ the full-potential Korringa-Kohn-Rostoker (FP-KKR) Green function method [37,38] as implemented in the SPR-TB-KKR code [39] to calculate the self-consistent electronic structure of the films and as implemented in the KKRIMP impurity-embedding code [40] for the electronic structure of the impurity adatoms.

Subsequently, we calculate the Bloch wave functions, the Fermi surfaces, and the scattering wave functions. From the latter, the scattering probability and the momentum- as well as the spin-flip relaxation rate can be quantitatively determined via the spin-dependent scattering matrix [20–24]. In this work, the spin-orbit coupling is added on top of the self-consistent scalar relativistic potential. Using this, the band structure, wave functions, and transition matrix are calculated in a "one-shot" way, i.e., without further self-consistency of the charge density (but still to all orders of the perturbation expansion with respect to SOC). After the calculations were finished we completed the development of a new approach [40] which enables us to treat the spin-orbit coupling plus full-potential self-consistently. The calculations for some test systems, e.g., Pt(111) and W(001) films, were repeated using the new approach and the results remained unchanged. Knowledge of the spin-dependent scattering probability allows us to employ the Boltzmann equation for spin Hall transport [12,41,42]. Then, the spin Hall conductivity as well as the spin Hall angle are calculated. The formalism that we use is already given in Refs. [23,40] and also partly in Refs. [25,29] of the authors. The most important expressions for making this paper self-contained are summarized in the following.

A. Elliott-Yafet parameter and the spin-flip scattering probability

The metallic films that we treat here exhibit time-reversal invariance (absence of external or internal magnetic fields) as well as space-inversion invariance (that holds for finite-thickness films in the bcc, fcc, or hcp crystal structure). Under these two symmetry-invariant conditions there are two orthogonal degenerate Bloch states at each $\mathbf{k}$ point in the band structure, $\Psi_{\mathbf{k}}^{+}$ and $\Psi_{\mathbf{k}}^{-}$, which can be written as superpositions of spin-up and -down states:

$$\begin{aligned}\Psi_{\mathbf{k}}^{+}(\mathbf{r}) &= [a_{\mathbf{k}}(\mathbf{r})|\uparrow\rangle + b_{\mathbf{k}}(\mathbf{r})|\downarrow\rangle]e^{i\mathbf{kr}},\\ \Psi_{\mathbf{k}}^{-}(\mathbf{r}) &= [a_{-\mathbf{k}}^{*}(\mathbf{r})|\downarrow\rangle - b_{-\mathbf{k}}^{*}(\mathbf{r})|\uparrow\rangle]e^{i\mathbf{kr}}.\end{aligned} \tag{1}$$

These two conjugate states show opposite spin polarization $\mathbf{S}_{\mathbf{k}}^{\pm} := \frac{\hbar}{2}\langle\Psi_{\mathbf{k}}^{\pm}|\boldsymbol{\sigma}|\Psi_{\mathbf{k}}^{\pm}\rangle$, i.e., $\mathbf{S}_{\mathbf{k}}^{+} = -\mathbf{S}_{\mathbf{k}}^{-}$. In an experiment, a spin-quantization axis (SQA) is defined by a unit vector $\hat{s}$ such that the injected spin population is polarized along $\hat{s}$. This situation is formally described by taking linear combinations of the two conjugate states at any $\mathbf{k}$ and forming new $\Psi_{\mathbf{k}}^{\pm}$ such that $\hat{s}\cdot\mathbf{S}_{\mathbf{k}}^{+}$ is maximized. It is then assumed, within the Elliott-Yafet approach, that the injected spins occupy these particular states $\Psi_{\mathbf{k}}^{+}$, while the spin-relaxation process occurs due to scattering from $\Psi_{\mathbf{k}}^{+}$ into $\Psi_{\mathbf{k}'}^{-}$. In this basis, where $\hat{s}\cdot\mathbf{S}_{\mathbf{k}}^{+}$ is maximized, the spin polarization is related to the coefficients $a_{\mathbf{k}}(\mathbf{r})$ and $b_{\mathbf{k}}(\mathbf{r})$ as follows:

$$a_{\mathbf{k}}^{2} := \int |a_{\mathbf{k}}(\mathbf{r})|^{2}\, d^{3}r = \frac{1}{2} + \frac{1}{\hbar}|\mathbf{S}_{\mathbf{k}}^{+}|, \tag{2}$$

$$b_{\mathbf{k}}^{2} := \int |b_{\mathbf{k}}(\mathbf{r})|^{2}\, d^{3}r = \frac{1}{2} - \frac{1}{\hbar}|\mathbf{S}_{\mathbf{k}}^{+}|, \tag{3}$$

where $|\mathbf{S}^+_{\mathbf{k}}| = \hat{s}\cdot\mathbf{S}^+_{\mathbf{k}}$ by the construction of the particular basis $\Psi^{\pm}_{\mathbf{k}}$. The Elliott-Yafet parameter $b^2_{\hat{s}}$ is defined as an average over the Fermi surface (FS)

$$b^2_{\hat{s}} := \langle b^2_{\mathbf{k}}\rangle_{\mathrm{FS}} = \frac{1}{n(E_{\mathrm{F}})}\frac{1}{V_{\mathrm{BZ}}}\int_{\mathrm{FS}}\frac{d\mathbf{k}}{\hbar|\mathbf{v}_{\mathbf{k}}|}b^2_{\mathbf{k}}, \tag{4}$$

where $\mathbf{v}_{\mathbf{k}}$ is the Fermi velocity and $n(E_{\mathrm{F}})$ is the density of states at the Fermi level. The subscript $\hat{s}$ indicates that the value of $b^2_{\hat{s}}$ depends on the choice of $\hat{s}$ through the dependence of $|\mathbf{S}^+_{\mathbf{k}}|$ (and thus of $b^2_{\mathbf{k}}$). Thus, we define the anisotropy of the EYP as

$$\mathcal{A}[b^2] = \frac{\max_{\hat{s}}\left(b^2_{\hat{s}}\right) - \min_{\hat{s}}\left(b^2_{\hat{s}}\right)}{\min_{\hat{s}}\left(b^2_{\hat{s}}\right)}. \tag{5}$$

As we have found in previous works [25,29,30,43], depending on the material, $\mathcal{A}\left[b^2\right]$ can reach large values, well exceeding 100%.

Within the Elliott approximation [15], where the form of the scattering potential is neglected and b^2 is assumed to be small, the spin-flip probability $P^{+-}_{\mathbf{k}\mathbf{k}'}$ is approximately proportional to $b^2_{\mathbf{k}}$. As a result, the ratio between the spin-flip relaxation rate T^{-1}_{sf} and the momentum-relaxation rate T^{-1}_{p} is proportional to the EYP, $T^{-1}_{\mathrm{sf}}/T^{-1}_{\mathrm{p}} \propto b^2$. This value depends on the electronic structure and the strength of spin-orbit coupling of the materials. Therefore, as we discuss later, it varies from Hf to Pt in the 5*d* group. For 5*d* transition metals with adatom defects, the assumptions of the Elliott approximation are certainly not valid. Still, the proportionality $T^{-1}_{\mathrm{sf}}/T^{-1}_{\mathrm{p}} \propto b^2$ holds qualitatively, as we discuss in Sec. III and show in Fig. 1.

B. Scattering off impurities

Now, we employ the scattering matrix to calculate the spin relaxation due to the impurity scattering. We use indices $\sigma,\sigma' \in \{+,-\}$ corresponding to the Bloch wave functions $\Psi^{\pm}_{\mathbf{k}}$ of Eq. (1). The wave functions scattered by the impurity at energy $E = E(\mathbf{k})$, $\Psi^{\mathrm{imp},\sigma}_{\mathbf{k}}(\mathbf{r})$, are calculated in terms of the unscattered Bloch wave functions of the host via the Lippmann-Schwinger equation

$$\Psi^{\mathrm{imp},\sigma}_{\mathbf{k}}(\mathbf{r}) = \Psi^{\sigma}_{\mathbf{k}}(\mathbf{r}) + \int d^3r' G(\mathbf{r},\mathbf{r}';E)\Delta V(\mathbf{r}')\Psi^{\mathrm{imp},\sigma}_{\mathbf{k}}(\mathbf{r}'). \tag{6}$$

The wave functions appearing here are column vectors in spin space. The host Green function $G(\mathbf{r},\mathbf{r}';E)$ is a 2×2 matrix in spin space. The same holds for ΔV, the difference between the impurity potential V^{imp} and the host potential including the difference of the spin-orbit contributions. The scattering matrix can be simply written in terms of the host and scattered wave functions

$$T^{\sigma\sigma'}_{\mathbf{k}\mathbf{k}'} = \int d^3r \left[\Psi^{\sigma}_{\mathbf{k}}(\mathbf{r})\right]^{\dagger}\Delta V(\mathbf{r})\,\Psi^{\mathrm{imp},\sigma'}_{\mathbf{k}'}(\mathbf{r}). \tag{7}$$

The integration in Eqs. (6) and (7) is numerically confined in the atomic cells where the difference in potential is found to be non-negligible. Under assumption of elastic scattering, the scattering probability due to a number of impurities in the system is determined by the golden rule

$$P^{\sigma\sigma'}_{\mathbf{k}\mathbf{k}'} = \frac{2\pi}{\hbar}Nc\left|T^{\sigma\sigma'}_{\mathbf{k}\mathbf{k}'}\right|^2\delta(E_{\mathbf{k}} - E_{\mathbf{k}'}), \tag{8}$$

where N is the number of atoms in the system and c is impurity concentration. Here, the concentration is defined as the number of impurities (adatoms) per surface unit cell and is therefore independent on the thickness of the film. The linear dependence of $P^{\sigma\sigma'}_{\mathbf{k}\mathbf{k}'}$ on the number of impurities cN implies that the scattering events are independent to each other and it is expected to hold in the dilute concentration limit where the defects do not form impurity bands. The $\mathbf{k}$-dependent relaxation rate can be calculated by summation over all $\mathbf{k}'$:

$$\left(\tau^{\sigma\sigma'}_{\mathbf{k}}\right)^{-1} = \sum_{\mathbf{k}'}P^{\sigma'\sigma}_{\mathbf{k}'\mathbf{k}} = \frac{2\pi Nc}{V_{\mathrm{BZ}}}\int_{\mathrm{FS}}\frac{d\mathbf{k}'}{\hbar^2|\mathbf{v}_{\mathbf{k}'}|}\left|T^{\sigma'\sigma}_{\mathbf{k}'\mathbf{k}}(E_{\mathrm{F}})\right|^2. \tag{9}$$

The relaxation rate averaged over the Fermi surface is obtained as

$$(\tau^{\sigma\sigma'})^{-1} = \frac{1}{n(E_{\mathrm{F}})}\frac{1}{V_{\mathrm{BZ}}}\int_{\mathrm{FS}}\frac{d\mathbf{k}}{\hbar|\mathbf{v}_{\mathbf{k}}|}\left(\tau^{\sigma\sigma'}_{\mathbf{k}}\right)^{-1}. \tag{10}$$

In a nonmagnetic system, it is obvious that $(\tau^{++})^{-1} = (\tau^{--})^{-1}$ which is the spin-conserving relaxation rate T^{-1}_{c} and $(\tau^{+-})^{-1} = (\tau^{-+})^{-1}$ which is the spin-flip relaxation rate T^{-1}_{sf}. The momentum-relaxation rate T^{-1}_{p} is then defined as $T^{-1}_{\mathrm{p}} = T^{-1}_{\mathrm{c}} + T^{-1}_{\mathrm{sf}}$ and the spin-relaxation rate T^{-1}_{1} is defined as two times the spin-flip relaxation rate $T^{-1}_{1} = 2T^{-1}_{\mathrm{sf}}$. The factor 2 appears since T_1 is experimentally derived from the full linewidth at half-amplitude of conduction electron resonance spectra.

Similar to the anisotropy of the EYP [Eq. (5)], we have a definition of the anisotropy of the spin-flip relaxation rate

$$\mathcal{A}\left[T^{-1}_{\mathrm{sf}}\right] = \frac{\max_{\hat{s}}T^{-1}_{\mathrm{sf}}(\hat{s}) - \min_{\hat{s}}T^{-1}_{\mathrm{sf}}(\hat{s})}{\min_{\hat{s}}T^{-1}_{\mathrm{sf}}(\hat{s})}. \tag{11}$$

To attest the numerical accuracy of the calculation of the relaxation time, the optical theorem

$$-\frac{2Nc}{\hbar}\mathrm{Im}T^{\sigma\sigma}_{\mathbf{k}\mathbf{k}} = \frac{2\pi N^2c}{V_{\mathrm{BZ}}\hbar}\sum_{\sigma'}\int_{\mathrm{FS}}\frac{d\mathbf{k}'}{\hbar|\mathbf{v}_{\mathbf{k}'}|}\left|T^{\sigma'\sigma}_{\mathbf{k}'\mathbf{k}}(E_{\mathrm{F}})\right|^2 \tag{12}$$

is also checked. In our calculations of thin metallic films, the optical theorem is very sensitive to the size of the vacuum region (number of empty-cell layers) and the approach to the real energy axis for the Green function $\lim_{\gamma\to 0}G(E_F + i\gamma)$. It is satisfied in most cases to within 5% and in few unfavorable cases, such as four-layer Pt(111) or four-layer Os(0001), to within 10%.

C. Spin Hall conductivity

To deal with the extrinsic spin Hall conductivity due to the skew scattering off impurities, the Boltzmann equation is utilized. The method was successfully applied to investigate the spin Hall effect in Cu and Au bulk as well as in Au(111) thin films with various impurities [12,41,42]. Following Refs. [12,41], we start from the linearized Boltzmann equation

for the mean-free path $\mathbf{\Lambda}$

$$\mathbf{\Lambda}^{\sigma}(\mathbf{k}) = \tau_{\mathbf{k}}^{\sigma}\left[\mathbf{v}_{\mathbf{k}} + \sum_{\mathbf{k}'\sigma'} P_{\mathbf{k}\mathbf{k}'}^{\sigma\sigma'}\,\mathbf{\Lambda}^{\sigma'}(\mathbf{k}')\right], \tag{13}$$

where $P_{\mathbf{k}\mathbf{k}'}^{\sigma\sigma'}$ is the scattering probability defined in Eq. (8) and the relaxation time $\tau_{\mathbf{k}}^{\sigma} = 1/\sum_{\sigma'}(\tau_{\mathbf{k}}^{\sigma\sigma'})^{-1}$ which is calculated from Eq. (9).

The term $\sum_{\mathbf{k}'\sigma'} P_{\mathbf{k}\mathbf{k}'}^{\sigma\sigma'}\mathbf{\Lambda}^{\sigma'}(\mathbf{k}')$ is called the scattering-in term and it can be separated into two parts: spin-conserving part when $\sigma' = \sigma$ and spin-flip part when $\sigma' \neq \sigma$. For the $5d$ materials that have the strong SOC, the spin-flip part cannot be neglected.

After self-consistently solving Eq. (13), the charge-conductivity tensor $\underline{\kappa}$ as well as the spin-conductivity tensor $\underline{\kappa}^{s}$ are determined as

$$\underline{\kappa} = \frac{e^2}{\hbar}\frac{1}{(2\pi)^2 d}\sum_{\sigma}\int_{\mathrm{FS}}\frac{d\mathbf{k}}{|\mathbf{v}_{\mathbf{k}}|}\mathbf{v}_{\mathbf{k}}\otimes\mathbf{\Lambda}^{\sigma}(\mathbf{k}) \tag{14}$$

and

$$\underline{\kappa}^{s} = \frac{e^2}{\hbar}\frac{1}{(2\pi)^2 d}\sum_{\sigma}\int_{\mathrm{FS}}\frac{d\mathbf{k}}{|\mathbf{v}_{\mathbf{k}}|}\left(\frac{2}{\hbar}S_{\mathbf{k}}^{z}\right)\mathbf{v}_{\mathbf{k}}\otimes\mathbf{\Lambda}^{\sigma}(\mathbf{k}), \tag{15}$$

respectively. $S_{\mathbf{k}}^{z}$ is the spin-expectation value calculated in Eqs. (2) and (3) by choosing the spin-polarization direction along the film normal meaning that the spin-quantization axis $\hat{s}$ is taken along the z direction. The expression for conductivity [Eqs. (14) and (15)] takes into account the film thickness d and can be directly compared to the conductivity in bulk. It is obvious that the charge and spin conductivities are inversely proportional to the impurity concentration. However, the ratio between them, the spin Hall angle $\alpha = \kappa^{s}/\kappa$, is independent of the impurity concentration.

D. General computational details

In our calculations, an angular momentum cutoff of $l_{\max} = 3$ is taken and the experimental lattice parameters are used for all elements. In order to obtain impurity wave functions [Eq. (6)] within the FP-KKR Green function method, the impurity potential is calculated using the Jülich KKR impurity-embedding code (KKRIMP) [40]. The charge- and spin-density screening of the impurity are self-consistently calculated within a cluster of nearest neighbors of the impurity atom. To test the influence of the cluster size, larger clusters of up to fourth-nearest neighbors are also considered in some cases showing negligible differences.

E. System of coordinates

For definiteness, we state here that throughout the paper we use the Cartesian structure coordinates of thin films xyz with respect to the bcc, fcc, or hcp structure basis. The following convention is used: the z axis is always the film normal and x and y axes are defined as the Cartesian coordinate related to the z axis, i.e., in fcc (001), bcc (001), or hcp (0001) films, the x and y directions are [100] and [010], respectively; in bcc (110) films, the x and y directions are [001] and $[1\bar{1}0]$, respectively; in fcc (111) films, the x and y directions are $[1\bar{1}0]$ and $[\bar{1}0\bar{1}]$, respectively.

F. Treatment of Rashba-type surface states

In many of the systems, surface states appear that obtain a Rashba character due to the spin-orbit coupling. Since the films in our calculations are symmetric, the Rashba states are double degenerate at each $E(\mathbf{k})$ with one state stemming from, and localized at, each film surface. Here, we should make two comments on their treatment.

First, in the doubly degenerate subspace we select $\Psi_{\mathbf{k}}^{+}$ and $\Psi_{\mathbf{k}}^{-}$ in the same way as for the bulklike states, i.e., by maximizing $b_{\mathbf{k}}^{2}$ along the given $\hat{s}$, instead of following the spin-orbit texture emerging from the Rashba effect. The motivation for this is that in the spin transport process we consider a thought experiment where conduction electrons are injected into the film with a pregiven spin direction $\hat{s}$, thus, we must use the same $\hat{s}$ in the analysis of all states. Generally, each of $\Psi_{\mathbf{k}}^{+}$ and $\Psi_{\mathbf{k}}^{-}$ will be a linear combination of true Rashba states with a given spin texture and may be localized simultaneously at both surfaces with a minimal intensity in the middle of the film.

Second, an *Ansatz* to distinguish the two degenerate true Rashba states in a way that reproduces their characteristic spin texture was presented in Ref. [29], Sec. IV. We summarize the idea here. Taking the twofold-degenerate subspace of the states at each $\mathbf{k}$ point, we can distinguish two orthogonal states by demanding that the spin-expectation value, integrated in one of the surface atomic layers, is maximal for the first state, and analogously in the other surface layer for the second state. As we discuss in Ref. [29], this *Ansatz* leads to the correct limit of surface-localized, spin-polarized Rashba states when the film thickness increases. Other possible *Ansätze*, e.g., maximizing the integrated charge density in the surface layer, lead to very similar results.

In this paper, we do not delve into a presentation of the spin texture occurring from our *Ansatz*. However, it is clear that the texture affects the spin-relaxation process. Consider for instance the scattering by adatoms. The position of the adatom on a particular surface automatically produces a preference of scattering of the state localized on the same surface merely by the larger overlap, and the spin transport will necessarily be affected by the spin texture of this state. These processes are of course implicit in our calculations.

III. RESULTS AND DISCUSSION

In order to systematically investigate the spin relaxation of $5d$ transition-metal thin films, we first calculate the EYP and discuss the results in Sec. III A. In Sec. III B, the momentum-relaxation time and spin-flip relaxation time due to scattering off self-adatom impurities are quantitatively analyzed. In Sec. III C, the spin Hall conductivity and spin Hall angle are studied. In order to compare results with free-electron-like metals, we also consider Au(111), Au(001), Cu(111), and Cu(001) thin films. We examine the behavior of the calculated quantities with respect to film thickness and orientation, and analyze them with respect to the Fermi surface, in particular concerning the surface states.

A. Elliott-Yafet parameter

According to the Elliott approximation, the calculation of the EYP can preliminarily describe the spin relaxation of the

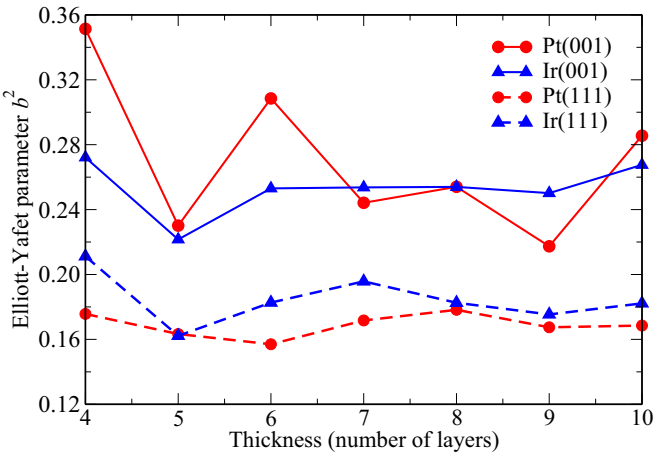

FIG. 2. (Color online) The thickness dependence of the Elliott-Yafet parameter in Pt(001), Pt(111), Ir(001), and Ir(111) thin films with the spin-quantization axis perpendicular to the films.

host materials. In a recent paper [29], we analyzed the EYP for bcc W(001) and discussed in detail its dependence on the film thickness. Remarkably, we found that owing to the surface states at the Fermi surface, the EYP of W(001) exhibits an oscillatory behavior with respect to the film thickness, which we traced back to the interaction of surface states at the two surfaces of the film together with the stacking of the bcc structure. In addition, the anisotropy of the EYP for W(001) thin films was found to have a high value of 37% at 10-layer film thickness. In this work, we present analogous calculations of the EYP for other 5*d* transition-metal thin films from Hf to Pt with different crystal structures.

First, we examine the film-thickness dependence of the EYP. In Fig. 2, we show the calculations of the EYP as a function of the film thickness for fcc Pt(001), Pt(111), Ir(001), and Ir(111) thin films with the SQA perpendicular to the films. These films are chosen since their EYPs show a variation with increasing the film thickness. In these systems, however, there are no surface states at the Fermi energy, which cause a pronounced oscillatory behavior of the EYP as found in W(001) films [29]. Yet, the influence from the stacking order along the z direction, i.e., . . .ABAB . . .in fcc (001) films and . . .ABCABC . . .in fcc (111) fims, could give rise to the fluctuation of the EYP due to the different boundary conditions (lateral shifting of the atoms) at different possible terminations. This is seen in Pt(001) and Pt(111). In the other 5*d* films, such as Ta(001), W(110), or the hcp metal (0001) surfaces, the variation of the EYP as a function of the film thickness is much smaller.

Shifting our attention to the EYP at a certain thickness of Pt and Ir films with the same crystalline orientation, we find that they are quantitatively very close. For instance, for 10-layer films, the EYP of Pt(001) and Ir(001) has a value of 0.286 and 0.268, respectively. In 10-layer Pt and Ir (111) films, they are both smaller than those of (001) thin films but have similar values of 0.168 and 0.182, respectively. It is also seen that the EYP of 0.184 for 10-layer hcp Os(0001) is very close to that of 0.187 for Re(0001). We summarize the values of the EYP for 5*d* films in 10-layer thickness in the first column of Table I.

For systems with Rashba surface states, the EYP can be very large, provided that the surface bands have a significant contribution to the density of states. For example, among the bcc thin films, W(001) and W(110) that have surface states at E_F have much higher EYP as compared to Ta(001) and Ta(110) which do not have the surface states. In 10-layer Hf(0001), the surface states at the Fermi surface also manifest in a large b^2 of 0.143 which is of the same magnitude as that of Os(0001) and Re(0001) films. To clarify the effect of the Rashba surface

TABLE I. Spin relaxation and spin Hall conductivity for 5*d* transition-metal 10-layer films, as well as Au and Cu, in different orientations. Ta and W are in the bcc structure, Ir, Pr, Au, and Cu in the fcc structure, and Hf, Re, and Os in the hcp structure (indicated in the first column). From left to right: the Elliott-Yafet parameter b^2 with the spin-quantization axis along the film normal z axis, and its anisotropy; the momentum-relaxation time T_p and the spin-flip relaxation time T_{sf} as well as the ratio between the spin-flip and the momentum-relaxation rates with the spin-quantization axis $\hat{s} \parallel z$ and the anisotropy of the spin-flip relaxation rate; the transverse spin conductivity in $(\mathrm{m}\Omega\,\mathrm{cm})^{-1}$, the charge conductivity in $(\mu\Omega\,\mathrm{cm})^{-1}$, the spin Hall angle α, and the existence of surface states at E_F (yes "y" or no "n").

Metal (surface)	b^2 $\hat{s} \parallel z$	$\mathcal{A}[b^2]$	T_p (ps at.%) $\hat{s} \parallel z$	T_{sf} (ps at.%) $\hat{s} \parallel z$	T_{sf}^{-1}/T_p^{-1} $\hat{s} \parallel z$	$\mathcal{A}[T_{sf}^{-1}]$	κ_{yx}^s $(\mathrm{m}\Omega\,\mathrm{cm})^{-1}$	κ_{xx} $(\mu\Omega\,\mathrm{cm})^{-1}$	$\alpha = \kappa_{yx}^s/\kappa_{xx}$ (%)	Surface states
Hf(0001) hcp	0.143	14%	0.120	0.372	0.322	97%	29.00	12.67	0.228	y
Ta(110) bcc	0.117	82%	0.146	0.676	0.215	57%	−12.90	22.98	−0.056	n
Ta(001) bcc	0.103	24%	0.319	1.836	0.174	13%	32.91	17.44	0.188	n
W(110) bcc	0.229	57%	0.085	0.220	0.384	71%	13.41	11.99	0.111	y
W(001) bcc	0.294	37%	0.088	0.208	0.422	27%	0.77	1.12	0.069	y
Re(0001) hcp	0.187	7%	0.108	0.280	0.386	8%	7.85	10.13	0.077	n
Os(0001) hcp	0.183	7%	0.097	0.248	0.394	10%	−12.59	18.09	−0.069	n
Ir(111) fcc	0.182	21%	0.168	0.504	0.332	3%	−26.91	27.22	−0.098	n
Ir(001) fcc	0.268	46%	0.123	0.300	0.409	20%	−5.42	10.34	−0.052	n
Pt(111) fcc	0.168	37%	0.392	1.078	0.363	12%	45.89	30.42	0.150	n
Pt(001) fcc	0.286	44%	0.411	0.986	0.416	7%	−17.14	16.41	−0.104	n
Au(111) fcc	0.036	11%	0.166	2.282	0.072	93%	−0.80	474.43	−0.002	y
Au(001) fcc	0.065	50%	0.160	5.974	0.026	48%	−71.03	217.28	−0.326	n
Cu(111) fcc	0.0016	11%	0.175	43.40	0.004	94%	−107.18	529.64	−0.020	y
Cu(001) fcc	0.0024	29%	0.159	515.0	0.0003	24%	−217.85	574.34	−0.037	n

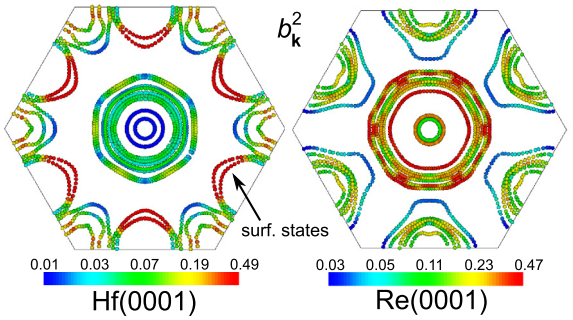

FIG. 3. (Color online) The distribution of $b^2_{\mathbf{k}}$ on the Fermi surfaces of 10-layer films of Hf(0001) (left) and Re(0001) (right). One of the surface states of Hf(0001) is pointed at by an arrow. The SQA is perpendicular to the films.

states, in Fig. 3, the distribution of $b^2_{\mathbf{k}}$ on the Fermi surface of 10-layer Hf and Re (0001) films is examined. One of the surface states of Hf(0001) is denoted by an arrow. It is obvious that in 10-layer Hf(0001) film the regions which provide a large contribution to b^2 are mainly distributed over the surface states. On the other hand, in 10-layer Re(0001) film, the complicated electronic structure with many crossing bands causes many spin-flip hot spots in the bulklike states. The surface-state-dependent effect is explained in Refs. [28,29] and one can apply the same arguments to state that the EYP is enhanced due to the existence of the Rashba surface states.

The EYP of 10-layer Au(111) and Au(001) films is one order of magnitude smaller, and the EYP of 10-layer Cu(111) and Cu(001) is even two orders of magnitude smaller than that of 5*d* transition metals. This demonstrates the important role of *d* states for spin-flip scattering promoted by strong mixing between spin-up and -down states. The complicated electronic structure with many band crossings in 5*d* thin films results in a large density of spin-flip hot spots which considerably enhance the spin-mixing parameter. As we calculated, the surface states of Au(111) and Cu(111) films have only a small contribution of about 5% to the DOS and thus their contribution to the total EYP is not dominant, i.e., 13% in 10-layer Au(111) and 19.5% in 10-layer Cu(111).

Now, we investigate the effect of the anisotropy of the EYP with respect to the SQA $\hat{s}$. In Fig. 4, the EYP is plotted for $\hat{s}$ on the unit sphere for 10-layer W(110) and 10-layer Os(0001) films, chosen as two opposite extremes among our data, in which the former shows a large value of anisotropy and the latter shows a small value. The EYP of a 10-layer W(110) film varies in a large range from 0.146 to 0.229, while the EYP of a 10-layer Os(0001) film varies in a smaller range from 0.171 to 0.183. As a result, an anisotropy $\mathcal{A}\left[b^2\right]$ of 57% for W(110) and 7% for Os(0001) is found. In addition, we calculated the anisotropy value for different film thickness. The results show that it is relatively robust with respect to the film thickness in some systems. For instance, it changes from 30% to 40% in Pt(111) or 20% to 30% in Ir(111) upon changing the thickness from 4 layers to 10 layers. On the other hand, for some systems, the anisotropy of EYP varies very much with film thickness. For example, it takes a value of 67% in four-layer W(110), and increases to a value of 113% in eight-layer W(110). Generally speaking, there is no theoretical limit for the anisotropy value.

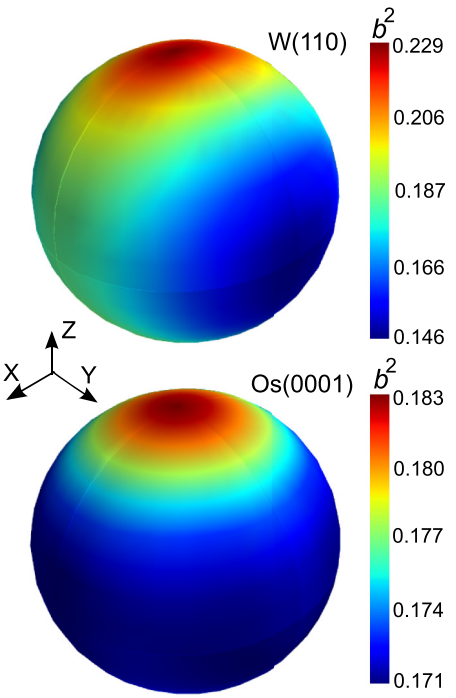

FIG. 4. (Color online) The value of b^2 of 10-layer W(110) and Os(0001) films for the spin-quantization axis $\hat{s}$ on the unit sphere.

However, one can see that it remains within the same order of magnitude if we change the thin-film thickness.

Only part of the difference between the two metals is due to surface states. In Fig. 5, the distribution of $b^2_{\mathbf{k}}$ on the Fermi surface of 10-layer W(110) film and 10-layer Os(0001) film is shown for the SQA along the z and x directions. One can see that, by rotating the SQA from the z axis to the x axis, the distribution of EYP in 10-layer W(110) film changes considerably not only at the surface states, but also at the bulklike states. On the contrary, the hot spots at the Fermi surface of 10-layer Os(0001) film remain when rotating the SQA.

In Refs. [25,29], we pointed out that the reduction of symmetry in thin films, compared to the bulk of cubic systems, will play a role for the anisotropy of the spin relaxation. One clear evidence for this can be seen in Fig. 4 in which the EYP of W(110) is maximal when $\hat{s}$ is parallel to the film normal. Moreover, the symmetry of EYP exactly corresponds to the crystallographic symmetry [25]. The anisotropy of the EYP of 57% in 10-layer W(110) that we find here is much larger as compared to 6% in bulk W [25]. The anisotropy values $\mathcal{A}[b^2]$ for other 10-layer films are summarized in the second column of Table I. Similar to W(110), other cubic films show a relatively high anisotropy value of the EYP as compared to almost negligible one in bulk materials. For example, 10-layer Ta(110) exhibits a large anisotropy of the EYP of 82% compared to 0.2% in bulk Ta. The anisotropy of 44% in Pt(001) is much larger than 0.4% in Pt bulk. It has to be noted that for all other films, the maximal value of the EYP is also obtained if the SQA is pointing perpendicular to the films.

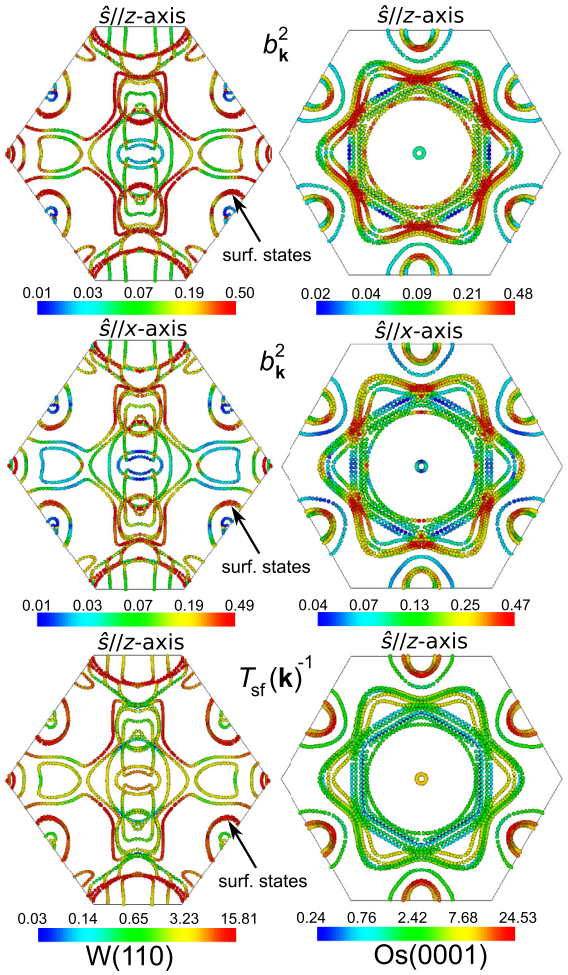

FIG. 5. (Color online) At the top and in the middle: the distribution of $b_{\mathbf{k}}^2$ on the Fermi surfaces of 10-layer W(110) (left) and Os(0001) films (right) for the SQA along the z axis (top) and x axis (middle). At the bottom: the distribution of $T_{\rm sf}(\mathbf{k})^{-1}$ on the Fermi surface of 10-layer W(110) film with W adatom defect (left) and 10-layer Os(0001) film with Os adatom defect (right) for the SQA along the z axis.

However, in the hcp case, the EYP shows a small anisotropy in thin films compared to the large value in bulk materials. For instance, the EYP of bulk Os shows an anisotropy of 59% [25], while it shows only a value of 7% in 10-layer Os(0001) film. The 10-layer Hf(0001) film shows only 14% of anisotropy of the EYP even though there are surface states at the Fermi surface. This is very small compared to the gigantic value of 830% of anisotropy of b^2 in bulk Hf [25]. In Refs. [25,43], we demonstrated that the spin-flip part of SOC depends strongly on the spin-quantization axis, at certain $\mathbf{k}$ points vanishing for one direction of the SQA while being maximal for another. In a rough approximation, we can imagine that the Fermi surface of thin films is constructed by the intersection of the Fermi surface of the bulk sample with a number of planes that are parallel to the film surface, with an interplane distance determined by the finite-size quantization of crystal momentum in the direction perpendicular to the film. Therefore, the spin-flip hot spots or hot areas that are formed at certain points in the bulk Fermi surface, e.g., at the hexagonal Brillouin zone edge [25], do not show in hcp(0001) film geometry unless the film becomes thick enough and the intersecting planes dense enough to capture these parts of the bulk Brillouin zone.

B. Spin relaxation due to self-adatom impurity

In this section, we discuss our results on the spin-relaxation process with self-adatoms as a source of scattering. The reason to choose adatom defects is that these naturally occur at any metal surface and additionally they comprise a reasonable generic model for surface roughness. Other scattering mechanisms (different defects or phonons at high temperature) would, of course, cause additional spin relaxation.

First of all, it is interesting to compare the quantities $b_{\mathbf{k}}^2$ and $\mathbf{k}$-dependent spin-flip relaxation rate $T_{\rm sf}(\mathbf{k})^{-1}$ distributed on the Fermi surfaces because in the spirit of the Elliott approximation, one expects a correlation between them. In the bottom of Fig. 5, the distribution of spin-flip relaxation rate on the Fermi surface of 10-layer W(110) (left) and Os(0001) (right) films with the SQA along the z direction are shown in comparison to $b_{\mathbf{k}}^2$ shown in the same figure. The $\mathbf{k}$ dependence of the spin-flip relaxation rate is obtained from the scattering rate in Eq. (9) as $T_{\rm sf}(\mathbf{k})^{-1} = (1/2)((\tau_{\mathbf{k}}^{+-})^{-1} + (\tau_{\mathbf{k}}^{-+})^{-1})$. Inspecting the color code of the two figures does not reveal a direct $\mathbf{k}$-dependent one-to-one correspondence between $b_{\mathbf{k}}^2$ and $T_{\rm sf}(\mathbf{k})^{-1}$. For instance, in W(110) the spin-relaxation rate at $\mathbf{k}$ points belonging to surface states is very high, while the value of $b_{\mathbf{k}}^2$ is not always high at the same positions. This also leads to a difference in the anisotropy value of b^2 and $T_{\rm sf}^{-1}$ that will be discussed later. A lack of direct correspondence between the values of $b_{\mathbf{k}}^2$ and $T_{\rm sf}(\mathbf{k})^{-1}$ is also found in Os(0001), where we see that the value of $b_{\mathbf{k}}^2$ at band crossings becomes almost maximal, while the value of $T_{\rm sf}(\mathbf{k})^{-1}$ at the same points is moderate compared to the half-rings on the outer part of the Brillouin zone. Our conclusion is that the Elliott approximation is too crude to give a correct impression about the $\mathbf{k}$-dependent spin relaxation, but, as we see below, it is qualitatively good for the $\mathbf{k}$-averaged quantities that are anyhow the ones measured by experiment.

Averaging over the Fermi surface, we obtain the spin-flip relaxation time $T_{\rm sf}$ as well as the momentum-relaxation time $T_{\rm p}$. The calculated results in ps-at.% for 10-layer films are presented in columns 3 and 4 of Table I. One can see that the systems with surface states, i.e., 10-layer W(001) and W(110) films, have short spin-flip and momentum-relaxation time as compared to others. For example, 10-layer W(110) film shows $T_{\rm p}$ of 0.085 ps-at.% and $T_{\rm sf}$ of 0.220 ps-at.% which are shorter than $T_{\rm p}$ of 0.146 ps-at.% and $T_{\rm sf}$ of 0.676 ps-at.% in 10-layer Ta(110) film. This is intuitively expected since the scattering takes place at the adatoms, with which surface states overlap more strongly than bulk states. The momentum-relaxation time of other 5d thin films is of the order of 0.1 to 0.4 ps-at.% and the spin-flip relaxation time is of the order of 0.3 to 1.8 ps-at.%. Comparing to the Au and Cu thin films, the momentum-relaxation time of 5d transition-metal thin films is in the same order of magnitude, however, the spin-flip relaxation time in 5d films is smaller by two or three orders of magnitude. It should be noted that the short spin-flip relaxation time of 5d thin films is also influenced strongly by the SOC of self-adatom impurity itself.

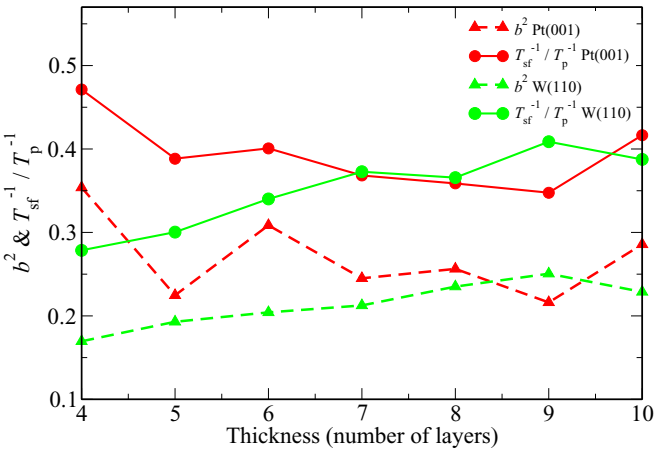

FIG. 6. (Color online) Thickness dependence of the ratio T_{sf}^{-1}/T_p^{-1} in Pt(001) and W(110) thin films with the self-adatom impurities.

An interesting question arises: How good is the Elliott approximation $T_{sf}^{-1}/T_p^{-1} \propto b^2$? To answer this, we report the ratio T_{sf}^{-1}/T_p^{-1} for 10-layer films and summarized in Table I. In addition, a comparison between the ratio T_{sf}^{-1}/T_p^{-1} and the EYP for a larger number of systems is shown in Fig. 1. Interestingly, although the value of spin-flip and momentum-relaxation rates varies very much among 5*d* transition-metal thin films, the ratio between them scales linearly, to a reasonable approximation, with the spin-mixing parameter. The prefactor 1.6 is obtained from a least-squares fitting, however, there is no clear reason for this value. This qualitative linear behavior is not obvious *a priori* since the Elliott approximation is based on the assumption of small values of $b_{\mathbf{k}}^2$ and also neglects the form of the scattering potential. Both assumptions should be too crude approximations for transition-metal adatoms on 5*d* films.

We can also examine the correlation between the ratio T_{sf}^{-1}/T_p^{-1} and the b^2 as a function of the film thickness. In fact, in our recent work on W(001) [29], we showed that the overall oscillating trend of T_{sf}^{-1}/T_p^{-1} with the film thickness corresponds well to an oscillation of the EYP. In Fig. 6, we show a similar plot where the ratio T_{sf}^{-1}/T_p^{-1} (solid lines) for Pt(001) (red) and W(110) (green) as well as the EYP (dashed lines) are shown as a function of the film thickness up to 10 layers (the SQA is taken perpendicular to the film). These two examples are chosen owing to the fact that in Pt(001), both T_{sf}^{-1}/T_p^{-1} and the EYP show a oscillatory behavior. In contrast, in W(110) both quantities show an increasing behavior with increasing the film thickness. Of course, there is no one-to-one correspondence between T_{sf}^{-1}/T_p^{-1} and the EYP in both films, but qualitatively they show the same trends. Once again, we can see the qualitative validity of the Elliott approximation.

The anisotropy of the spin-flip relaxation rate is also investigated in relation to the crystal symmetry by changing the spin-polarization direction. In Fig. 7, we show $T_{sf}^{-1}(\hat{s})$ for 10-layer W(110) and Os(0001) films with the spin-quantization axis $\hat{s}$ on the unit sphere. Similarly to the case of the EYP, the maximum value of T_{sf}^{-1} is obtained for $\hat{s}$ out of plane. However, there is no one-to-one correspondence between the anisotropy of spin-flip relaxation rate and the EYP.

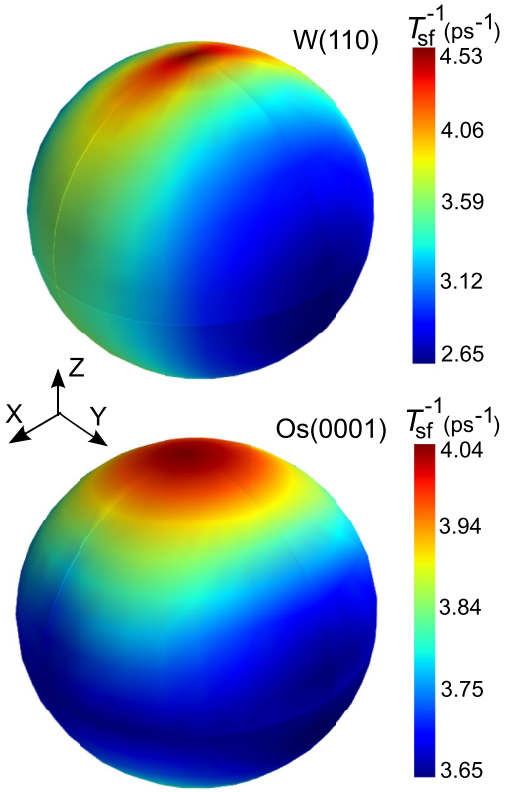

FIG. 7. (Color online) The spin-flip relaxation rate T_{sf}^{-1} in ps^{-1}/at.% of 10-layer W(110) film with W adatom and of 10-layer Os(0001) film with Os adatom as scatterers as a function of the spin-quantization axis $\hat{s}$ on the unit sphere.

The calculated $\mathcal{A}[T_{sf}^{-1}]$ in 10-layer films is also shown in Table I. The anisotropy of 10-layer Cu(111), Cu(001), Au(111), and Au(001) films is also calculated for comparison. It can be seen that in the films with surface states, such as 10-layer W(110), Hf(0001), Au(111), and Cu(111) films with self-adatom impurity, the anisotropy value of the spin-flip relaxation rate is surprisingly higher as compared to that of the EYP. In particular, in 10-layer Hf(0001) film, it reaches as mush as 97%. We can analyze this by examining $T_{sf}(\mathbf{k})^{-1}$ on the Fermi surface of 10-layer Hf(0001) film with self-adatoms as scatterers in Fig. 8. Indeed, the $T_{sf}^{-1}(\mathbf{k})$ at the surface states with $\hat{s} \parallel z$ exhibits high values and it is much lower for $\hat{s} \parallel x$. As shown in Fig. 5 for W(110) with W adatom impurity, $T_{sf}(\mathbf{k})^{-1}$ has also very high values at the surface states. We can infer that the anisotropy of the spin-flip relaxation rate is highly increased due to the Rashba surface states because of their preferential, **k**-dependent spin polarization (i.e., their Rashba character) and because, as surface states, they have a strong overlap with the adatom scatterers.

The anisotropy value of the spin-flip relaxation rate in other 10-layer thin films with self-adatom impurities as scatterers and without surface states is comparable to that of the EYP. The cubic systems show a high anisotropy of spin-flip relaxation rate such as 57% in Ta(110) with Ta adatom impurity or 48% in Au(001) with Au adatom impurity. However, similar to the anisotropy of EYP, the hcp thin films show a small value $\mathcal{A}[T_{sf}^{-1}] = 10\%$ in Os(0001) and 8% in Re(0001). This result

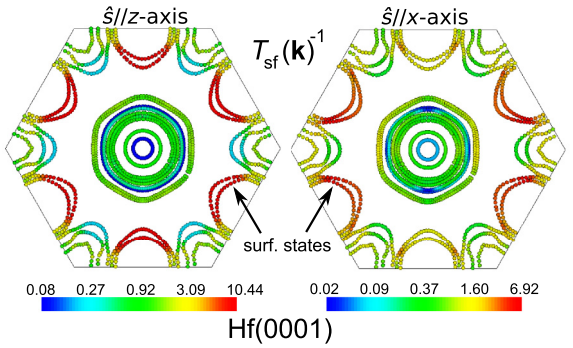

FIG. 8. (Color online) The distribution of spin-flip relaxation rate $T_{sf}(\mathbf{k})^{-1}$ in ps^{-1}/at.% on the Fermi surface of 10-layer Hf(0001) film with Hf adatom defect in the cases of the spin-quantization axis $\hat{s} \parallel z$ (left) and $\hat{s} \parallel x$ (right). Surface states are indicated by arrows.

is expected and it can be explained in a similar way for the anisotropy of the EYP. As discussed in Refs. [25,29,30,43], there is no theoretical limit on the value of anisotropy and, as a consequence, this value depends very much on the material parameters.

C. Spin Hall conductivity

We proceed with an investigation of the extrinsic spin Hall conductivity due to skew scattering off self-adatoms. Assuming that we set the x direction as the charge current direction and the z direction as the spin-polarization direction, the central experimentally accessible quantity in the spin Hall effect is the spin Hall angle $\alpha = \kappa^s_{yx}/\kappa_{xx}$ relating the transverse spin current to the longitudinal charge current. κ^s_{yx} and κ_{xx} are the off-diagonal elements of the spin-conductivity tensor [Eq. (15)] and the diagonal elements of the charge-conductivity tensor [Eq. (14)], respectively.

First, we note on the anisotropy of spin Hall angle with respect to the current direction in bcc (110) films. From the conductivity tensor, in principle, we can have two definitions of spin Hall angle depending on the direction of the longitudinal current. The spin Hall angle defined above corresponds to the electric field applied along the x axis. We can also apply an electric field along the y axis, which will result in the following value for the spin Hall angle $\alpha' = -\kappa^s_{xy}/\kappa_{yy}$ as measured experimentally. In case of a high in-plane symmetry, which is the case for, e.g., W(001) films, $\alpha = \alpha'$, while when the in-plane symmetry is lowered, e.g., W(110) and Ta(110) films, the spin Hall angles α and α' can be different from each other. In Fig. 9, the spin Hall angles α and α' of W(110) with W adatom as scatterer and Ta(110) with Ta adatom as scatterer are plotted as a function of the film thickness. It can be seen that the spin Hall angles can vary very much. In many cases, even the sign of the SHA α and α' is different. This leads to a high anisotropy effect of the spin Hall angle in such systems with respect to the current direction. As seen in Fig. 9, the anisotropy can reach up to 300% in eight-layer W(110) film or 200% in seven-layer Ta(110) film. The high values of anisotropy of spin Hall angle come from the anisotropy in both spin and charge current. One should stress that the anisotropy of SHA here is with respect to the current direction in the film and it is in contrast to the EYP and spin-relaxation case where we

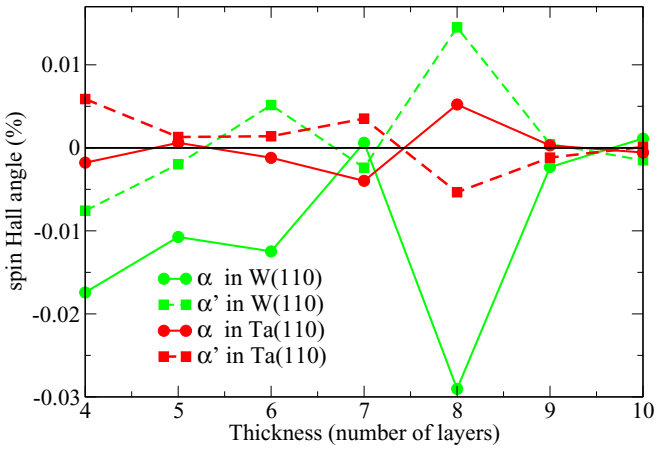

FIG. 9. (Color online) Spin Hall angles $\alpha = \kappa^s_{yx}/\kappa_{xx}$ and $\alpha' = -\kappa^s_{xy}/\kappa_{yy}$ of W(110) with W adatom impurity and Ta(110) with Ta adatom impurity as a function of the film thickness. The definition of the x and y directions is presented in Sec. IIE.

observed an anisotropy with respect to the spin-polarization direction $\hat{s}$.

It is also rewarding to observe that the spin Hall angle oscillates with increasing film thickness. In Fig. 10, the spin Hall angle $\alpha = \kappa^s_{yx}/\kappa_{xx}$ is shown as a function of film thickness for W(001) and Pt(111) with self-adatom impurities. From the definition of the spin Hall angle, one can expect an independence of α on the film thickness. However, in both cases, the spin Hall angle shows an oscillatory dependence on the film thickness, indicating quantum confinement effect [42]. We have previously seen oscillatory effects also in the EYP and the spin-flip relaxation rate of W(001) films and Pt(111) films as a function of thickness shown in Ref. [29] as well as in this work. However, the variation curve of spin Hall angle is different from that of the EYP or the spin relaxation. In fact, a correspondence between the spin-flip relaxation rate and the spin Hall angle is not expected: as can be seen from the scattering-in term in Eq. (13), the spin Hall conductivity

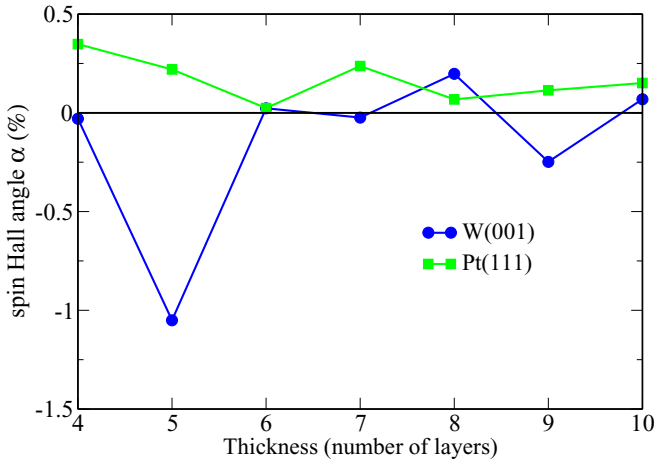

FIG. 10. (Color online) Spin Hall angle α of W(001) with W adatom defect and Pt(111) with Pt adatom defect as a function of the film thickness.

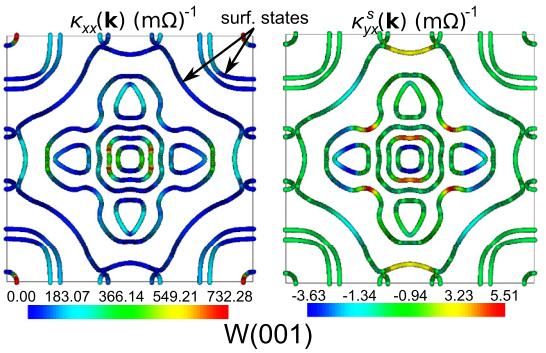

FIG. 11. (Color online) The distribution of the charge conductivity $\kappa_{xx}(\mathbf{k})$ and the transverse spin conductivity $\kappa^s_{yx}(\mathbf{k})$ in (milliOhm)$^{-1}$ on the Fermi surface of 10-layer W(001) film with 1% self-adatom impurities.

is determined by the contributions of the spin-conserving and spin-flip probabilities, while the spin-flip relaxation is determined only by the spin-flip probability.

We investigate the effect in more detail by plotting the distribution of the charge and transverse spin conductivty on the Fermi surface of 10-layer W(001) film with 1% self-adatom impurities in Fig. 11. Quantities $\kappa_{xx}(\mathbf{k})$ and $\kappa^s_{yx}(\mathbf{k})$ are simply defined as $\mathbf{k}$ distributions of the charge and spin conductivities on the Fermi surface $\kappa^{(s)}_{xx(yx)} = \int_{\mathrm{FS}} d\mathbf{k} \cdot \kappa^{(s)}_{xx(yx)}(\mathbf{k})$ and the unit of $\kappa(\mathbf{k})$ is (milliOhm)$^{-1}$ [cf. also Eqs. (14) and (15)]. Obviously, the bulklike states carry most of the longitudinal charge current and the surface states do not, i.e., the charge conductivity is very low at surface states. On the contrary, one can expect that the surface states can carry a transverse spin current due to the very strong scattering [42]. However, it is not the case for this system. Large transverse spin conductivities are also seen in the bulklike states.

Table I summarizes the charge and spin conductivity as well as the spin Hall angle α of 5d 10-layer films together with 10-layer Au and Cu. The impurity concentration is 1% for all calculations. The values for W(110) and Ta(110) films are illustrated with $\alpha = \kappa^s_{yx}/\kappa_{xx}$ (as opposed to $\alpha' = -\kappa^s_{xy}/\kappa_{yy}$, see discussion in the beginning of this section). A first impression is that the spin Hall angles are rather small in magnitude for all systems. Moreover, they are quite different in magnitude and sign when changing the material. We also examined if the Rashba surface states influence the spin Hall angle due to large scattering strength. Our calculations show rather small spin Hall angles in films with surface states. For example, 10-layer W(001) film with W adatom impurity shows only a value of 0.06% for spin Hall angle, while its value in 10-layer Au(111) film with Au adatom impurity is very small constituting only -0.0017%. Comparing between Cu films and 5d transition-metal films with different strength of SOC, we can observe no clear trend in the magnitude of the spin Hall angle with increasing the SOC strength.

IV. SUMMARY

In this work, we studied the consequences of spin-dependent scattering in nonmagnetic metallic thin films. We particularly focused on the effects of the spin relaxation induced by the Elliott-Yafet mechanism as well as the extrinsic spin Hall transport due to the skew scattering for 5d transition-metal thin films with self-adatom impurity in comparison with Au and Cu thin films.

The Elliott-Yafet parameter and the spin relaxation are systematically examined as functions of the film thickness up to 10 layers as well as the crystallographic orientation of the film. The overall trends are in qualitative agreement with the Elliott approximation. Quantitatively, due to strong spin-flip scattering and complicated electronic structure in d-orbital materials, the spin-flip relaxation time of 5d transition metals with self-adatom impurity is roughly about few hundred nanoseconds at atomic percent which is two or three orders of magnitude shorter than that of Cu and Au thin films.

Owing to the reduced dimensionality, the anisotropy of the spin-mixing parameter and the spin-flip relaxation rate in thin films is different from that in bulk metals, but not in a universal manner. For cubic crystal structures, the anisotropy significantly increases in thin films compared to that in bulk systems because of the crystal-symmetry reduction. On the contrary, in hcp materials where the symmetry in bulk is anyhow low, the anisotropy value in bulk is quite large and in all studied cases higher than the value in thin films, as a result of the Fermi surface formation. Furthermore, we find that the presence of Rashba surface states plays a crucial role in the spin relaxation. For example, the anisotropy of spin-flip relaxation rate reaches a value of 97% in 10-layer Hf(0001) or 71% in 10-layer W(110) films. Although they enhance the EYP and the spin-flip scattering, their overall contribution can be large or small compared to the contribution of the bulklike states, depending on the system. An important factor here is the relative contribution of the Rashba states to the total DOS.

The longitudinal charge conductivity and the transverse spin Hall current for 10-layer thin films with 1% self-adatom impurities are calculated by means of the self-consistent Boltzmann equation. The spin Hall angle found to strongly vary in 5d films with respect to the material but also with respect to film thickness and orientation.

ACKNOWLEDGMENTS

This work was financially supported by Deutsche Forschungsgemeinschaft Projects No. MO 1731/3-1 and No. SPP 1538 SpinCaT, and the HGF-YIG NG-513 project of the Helmholtz Gemeinschaft. The authors are grateful to G. Bihlmayer, R. Zeller, and P. Dederichs for fruitful discussions. We acknowledge computing time on the supercomputers JUQEEN and JUROPA at Jülich Supercomputing Center and JARA-HPC of RWTH Aachen University.

[1] S. A. Wolf, D. D. Awschalom, R. A. Burhmanm, J. M. Daughton, S. von Molnar, M. L. Roukes, A. Y. Chtchelkanova, and D. M. Treger, Science **294**, 1488 (2001).

[2] S. S. P. Parkin, in *Spin Dependent Transport in Magnetic Nanostructures*, edited by S. Maekawa and T. Shinjo (Taylor and Francis, New York, 2002).

[3] I. Zutic, J. Fabian, and D. Sarma, Rev. Mod. Phys. **76**, 323 (2004).

[4] M. Johnson and R. H. Silsbee, Phys. Rev. Lett. **55**, 1790 (1985).

[5] M. Johnson and R. H. Silsbee, Phys. Rev. B **37**, 5326 (1988).

[6] T. Kimura, J. Hamrle, and Y. Otani, Phys. Rev. B **72**, 014461 (2005).

[7] E. Beaurepaire, J. C. Merle, A. Daunois, and J. Y. Bigot, Phys. Rev. Lett. **76**, 4250 (1996).

[8] J. E. Hirsch, Phys. Rev. Lett. **83**, 1834 (1999).

[9] Y. K. Kato, R. C. Mayers, A. C. Gossard, and D. D. Awschalom, Science **306**, 1910 (2004).

[10] S. O. Valenzuela and M. Tinkham, Nature (London) **442**, 176 (2006).

[11] T. Seki, Y. Hasegawa, S. Mitani, S. Takahashi, H. Imamura, S. Maekawa, J. Nitta, and K. Takanashi, Nat. Mater. **7**, 125 (2008).

[12] M. Gradhand, D. V. Fedorov, P. Zahn, and I. Mertig, Phys. Rev. Lett. **104**, 186403 (2010).

[13] E. Saitoh, M. Ueda, H. Miyajima, and G. Tatara, Appl. Phys. Lett. **88**, 182509 (2006).

[14] T. Kimura, Y. Otani, T. Sato, S. Takahashi, and S. Maekawa, Phys. Rev. Lett. **98**, 156601 (2007).

[15] R. J. Elliott, Phys. Rev. **96**, 266 (1954).

[16] Y. Yafet, in *Solid State Physics*, edited by F. Seitz and D. Turnbull (Academic, New York, 1963), Vol. 14, p. 1.

[17] H. A. Kramers, Proc. Amsterdam Acad. **33**, 959 (1930).

[18] J. Fabian and S. Das Sarma, Phys. Rev. Lett. **81**, 5624 (1998).

[19] V. P. Zhukov, E. V. Chulkov, and P. M. Echenique, Phys. Status Solidi A **205**, 1296 (2008).

[20] D. V. Fedorov, P. Zahn, M. Gradhand, and I. Mertig, Phys. Rev. B **77**, 092406 (2008).

[21] M. Gradhand, M. Czerner, D. V. Fedorov, P. Zahn, B. Y. Yavorsky, L. Szunyogh, and I. Mertig, Phys. Rev. B **80**, 224413 (2009).

[22] M. Gradhand, D. V. Fedorov, F. Pientka, P. Zahn, I. Mertig, and B. L. Györffy, Phys. Rev. B **84**, 075113 (2011).

[23] S. Heers, Ph.D. Thesis, RWTH Aachen University, 2011; http://darwin.bth.rwth-aachen.de/opus3/volltexte/2011/3827/

[24] S. Heers, P. Mavropoulos, S. Lounis, R. Zeller, and S. Blügel, Phys. Rev. B **86**, 125444 (2012).

[25] B. Zimmermann, P. Mavropoulos, S. Heers, N. H. Long, S. Blügel, and Y. Mokrousov, Phys. Rev. Lett. **109**, 236603 (2012).

[26] E. I. Rashba, Fiz. Tver. Tela (Leningrad) **2**, S. 1224 (1960) [Sov. Phys. Solid State **2**, 1109 (1960)].

[27] O. Krupin, G. Bihlmayer, K. Starke, S. Gorovikov, J. E. Prieto, K. Döbrich, S. Blügel, and G. Kaindl, Phys. Rev. B **71**, 201403(R) (2005).

[28] N. Miyata, H. Narita, M. Ogawa, A. Harasawa, R. Hobara, T. Hirahara, P. Moras, D. Topwal, C. Carbone, S. Hasegawa, and I. Matsuda, Phys. Rev. B **83**, 195305 (2011).

[29] N. H. Long, P. Mavropoulos, B. Zimmermann, S. Heers, D. S. G. Bauer, S. Blügel, and Y. Mokrousov, Phys. Rev. B **87**, 224420 (2013).

[30] N. H. Long, P. Mavropoulos, S. Heers, B. Zimmermann, Y. Mokrousov, and S. Blügel, Phys. Rev. B **88**, 144408 (2013).

[31] P. Gambardella, S. Rusponi, M. Veronese, S. S. Dhesi, C. Grazioli, A. Dallmeyer, I. Cabria, R. Zeller, D. H. Dederichs, K. Kern, C. Carbone, and H. Brune, Science **300**, 1130 (2003).

[32] M. M. Soares, M. De Santis, H. C. N. Tolentino, A. Y. Ramos, M. El Jawad, Y. Gauthier, F. Yildiz, and M. Przybylski, Phys. Rev. B **85**, 205417 (2012).

[33] U. Gradmann, M. Przybylski, H. J. Elmers, and G. Liu, Appl. Phys. A **49**, 563 (1989).

[34] B. Dupe, M. Hoffmann, C. Paillard, and S. Heinze, Nat. Commun. **5**, 4030 (2014).

[35] F. J. Jedema, A. T. Filip, and B. J. van Wees, Nature (London) **410**, 345 (2001).

[36] S. H. Vosko, L. Wilk, and M. Nusair, Can. J. Phys. **58**, 1200 (1980).

[37] N. Papanikolaou, R. Zeller, and P. H. Dederichs, J. Phys.: Condens. Matter **14**, 2799 (2002); H. Ebert, D. Kdderitzsch, and J. Minár, Rep. Prog. Phys. **74**, 096501 (2011); see also http://www.kkr-gf.org

[38] N. Stefanou and R. Zeller, J. Phys.: Condens. Matter **3**, 7599 (1991); N. Stefanou, H. Akai, and R. Zeller, Comput. Phys. Commun. **60**, 231 (1990).

[39] H. Ebert and R. Zeller, http://olymp.cup.uni-muenchen.de/ak/ebert/SPR-TB-KKR

[40] D. S. G. Bauer, Ph.D. thesis, RWTH Aachen University, 2014; http://darwin.bth.rwth-aachen.de/opus3/volltexte/2014/4925/

[41] I. Mertig, Reg. Prog. Phys. **62**, 237 (1999).

[42] C. Herschbach, M. Gradhand, D. V. Fedorov, and I. Mertig, Phys. Rev. B **85**, 195133 (2012).

[43] Y. Mokrousov, H. Zhang, F. Freimuth, B. Zimmermann, N. H. Long, J. Weischenberg, I. Souza, P. Mavropoulos, and S. Blügel, J. Phys.: Condens. Matter **25**, 163201 (2013).